RSC Advances

PAPER

View Article Online
View Journal | View Issue

Cite this: *RSC Adv.*, 2025, **15**, 19348

Tunable color, optical properties, and energy transfer of Tb^{3+}–Sm^{3+}–Yb^{3+} tri-doped lithium–niobium–tellurite glass for applications in color display devices and WLEDs†

Ho Kim Dan, *[ab] Nguyen Dinh Trung,[c] Nguyen Minh Tam, [d] L. T. Ha,[e] Vu Thi Kim Lien,*[fg] D. T. Khan,[h] Nguyen Le Thai,[i] Dacheng Zhou[j] and Jianbei Qiu[j]

A TeO_2–Nb_2O_5–LiO_2–CaO (TNLC) lithium–niobium–tellurite glass single-doped and co-doped with Tb^{3+}, Sm^{3+}, and Yb^{3+} ions was synthesized *via* a conventional melt-quenching method. The Tb^{3+}–Sm^{3+} co-doped TNLC glass could be tuned to emit white light effectively by controlling the ratio of Tb^{3+} and Sm^{3+} in the glass. The fluorescence lifetime of the Tb^{3+}–Sm^{3+} co-doped TNLC glass indicated the existence of multiple energy transfer channels, including from Tb^{3+} to Sm^{3+} ions and the reverse energy transfer from Sm^{3+} to Tb^{3+} ions. Taking advantage of these energy transfer channels, the color coordinates of the material could be changed from yellowish-pink and yellowish-green emissions to white emission by controlling the ratio of ions doped in TNLC glasses. The optimal molar concentration ratio between Tb^{3+} and Sm^{3+} ions for the best white light emission was 0.83 for the TNLC-0.5Tb0.6Sm sample. Changing the ratio of these rare-earth (RE) ions allowed tuning the color temperature of the material from 5616 to 7699 K. Thus, Tb^{3+}–Sm^{3+} co-doped and Tb^{3+}–Sm^{3+}–Yb^{3+} tri-doped TNLC glasses are promising materials for color display applications and white light-emitting diodes (WLEDs).

Received 15th April 2025
Accepted 4th May 2025

DOI: 10.1039/d5ra02624e

rsc.li/rsc-advances

1. Introduction

In recent years, with the rapid development and high demand of optoelectronic materials for color display technologies and devices,[1,2] light-emitting diodes (LEDs)[3,4] that emit in the visible region, display full colors and are color-tunable are in high demand, promoting extensive research on rare-earth (RE)-ion doping in various host matrices,[5–7] such as phosphors, glasses, and glass-ceramic containing nanocrystals. Among various host matrices, tellurite-based glasses have emerged as promising candidates owing to their unique physicochemical and optical properties.[5,6] Tellurite-based glasses have a relatively low melting point, high thermal stability, good RE ion solubility, a wide transmission window (covering the visible (VIS) to near-infrared (NIR) region), and low phonon energy (which minimizes non-radiative (NR) losses and enhances emission efficiency).[7,8] Co-doping RE ions in tellurite glasses facilitates sharp, well-defined intra-4f electronic transitions that result in highly stable and efficient luminescence. The incorporation of RE ions in tellurite glasses further opens up pathways for energy transfer (ET) interactions, enabling the tuning of emission intensity and chromaticity of color in the visible wavelength range.[9,10] The combination of Sm^{3+}, Tb^{3+}, and Yb^{3+} ions produces a cooperative, energy-transferring, and tunable emission intensity and colorimetry for visible and upconversion (UC) emissions when excited at different wavelengths.[11] Sm^{3+} ions exhibit prominent orange-red emission around 600–650 nm, corresponding to $^4G_{5/2} \rightarrow {}^6H_{7/2}$ and $^4G_{5/2} \rightarrow {}^6H_{5/2}$ transitions;[12,13] Tb^{3+} ions produce strong green emission near 546 nm, corresponding to $^5D_4 \rightarrow {}^7F_5$ transition,[14,15] and Yb^{3+} ions exhibit only one $^2F_{5/2} \rightarrow {}^2F_{7/2}$ transition and acts as a sensitizer owing to their strong absorption at ~980 nm and the ability to participate in UC and cross-relaxation (CR)

[a]*Optical Materials Research Group, Science and Technology Advanced Institute, Van Lang University, Ho Chi Minh City, Vietnam. E-mail: hokimdan@vlu.edu.vn*
[b]*Faculty of Applied Technology, School of Technology, Van Lang University, Ho Chi Minh City, Vietnam*
[c]*Faculty of Chemistry and Environment, Dalat University, Lam Dong, Vietnam*
[d]*Faculty of Basic Sciences, University of Phan Thiet, 225 Nguyen Thong, Phan Thiet City, Binh Thuan, Vietnam*
[e]*Institute of Science and Technology, TNU-University of Sciences, Thai Nguyen 250000, Vietnam*
[f]*Institute of Theoretical and Applied Research, Duy Tan University, Hanoi 100000, Vietnam. E-mail: vutkimlien@duytan.edu.vn*
[g]*Faculty of Natural Sciences, Duy Tan University, Da Nang 550000, Vietnam*
[h]*The University of Danang, University of Science and Education, Da Nang, 550000, Vietnam*
[i]*Faculty of Engineering and Technology, Nguyen Tat Thanh University, Ho Chi Minh City, Vietnam*
[j]*Key Laboratory of Advanced Materials of Yunnan Province, Kunming University of Science and Technology, Kunming 650093, China*

† Electronic supplementary information (ESI) available. See DOI: https://doi.org/10.1039/d5ra02624e

mechanisms.[16,17] Some works have explored the color tunability, luminescence properties, and ET mechanisms in RE ion co-doped glasses/glass ceramics to develop materials suitable for color display and LED applications.[18–20] F. Nawaz *et al.*[21] investigated and reported the influence of Yb^{3+} co-doping on the optical properties of Sm^{3+}-doped sodium tellurite glasses. They found that Yb^{3+} co-doping affected the absorption and emission characteristics of Sm^{3+} ions, indicating ET between the Sm^{3+} and Yb^{3+} ions.[21] J. Li *et al.*[22] reported a multi-color afterglow in Tb^{3+}–Sm^{3+} co-doped gallo-silicate glass ceramics. By adjusting the concentrations of Tb^{3+} and Sm^{3+} ions, the afterglow emission could be tuned from green to orange and then to yellow.[22] This study highlighted ET and trap-sharing mechanisms between the dopants, which are significant for optical anti-counterfeiting applications. In general, these studies collectively enhance our understanding of ET dynamics and luminescence tuning in RE co-doped tellurite glass systems, contributing to the development of materials for color displays, LEDs, and other photonic applications.[21,22]

Lithium–niobium–tellurite (Li–Nb–Te) glass is particularly advantageous as a host because the incorporation of lithium and niobium oxides enhances the structural network,[23] improves RE ion dispersion, and increases the optical bandgap and nonlinear optical properties. The presence of Nb^{5+} ions, which act as a glass modifier, can influence local field symmetry and aid the creation of non-centrosymmetric sites that are beneficial for RE ion emission.[23,24] Furthermore, the addition of Li_2O serves to improve glass formability and optical clarity while also aiding ET dynamics by modifying the local coordination environment of the RE ions.[25] Although several studies have explored tellurite glasses single-doped and co-doped with Tb^{3+}, Sm^{3+}, and Yb^{3+} ions, as well as other optical materials containing these RE ions, most of them have focused on ET mechanisms from Tb^{3+} to Sm^{3+} ions. However, reverse ET mechanisms, such as from Sm^{3+} to Tb^{3+} ions or from Yb^{3+} to both Tb^{3+} and Sm^{3+} ions, have not been reported. These mechanisms are crucial for enabling strong visible emission under 980 nm infrared excitation, corresponding to the transition of Yb^{3+} from the $^2F_{7/2}$ to $^2F_{5/2}$ state. In this study, TeO_2–Nb_2O_5–Li_2O–CaO (TNLC) glasses with various doping schemes, including Tb^{3+}-doped, Sm^{3+}-doped, Tb^{3+}–Sm^{3+} co-doped, and Tb^{3+}–Sm^{3+}–Yb^{3+} tri-doped glasses, were synthesized *via* melt-quenching. We investigated the effect of varying the concentrations of these ions on the emission color. A detailed analysis of the ET processes from Tb^{3+} to Sm^{3+}, Sm^{3+} to Tb^{3+}, and Yb^{3+} to both Tb^{3+} and Sm^{3+} ions was conducted. By adjusting the ion ratios, white-light emission was achieved. These findings suggest that TNLC glasses co-doped with Tb^{3+}, Sm^{3+}, and Yb^{3+} ions are promising candidates for color display technologies and white light-emitting diodes (LEDs).

2. Experimental details

The lithium–niobium–tellurite glasses used in this work were synthesized using a conventional melt-quenching technique. High-purity laboratory-grade reagents (99.99%), including TeO_2, Nb_2O_5, Li_2O, CaO, TbF_3, Sm_2O_3, and Yb_2O_3, were used as raw materials. Specific compositions, molar ratios, and corresponding sample abbreviations are summarized in Table 1.

Approximately 12 grams of each glass batch was prepared by accurately weighing the required mixtures of raw materials using an electronic analytical balance. After finely grinding them using an onyx mortar and agate pestle, the mixtures were compacted, placed in a platinum crucible and then heated in a Nabertherm electric furnace (Germany) at 1150 °C for 45 minutes under an air atmosphere.[16,26,27] Following the melting process, the molten materials were cast into molds and rapidly cooled on a stainless-steel plate to form the initial glass

Table 1 Specific glass compositions and molar concentration ratios of the as-synthesized TeO_2–Nb_2O_5–LiO_2–CaO–TbF_3–Sm_2O_3–Yb_2O_3 lithium–niobium–tellurite glasses

	Molar concentration ratio of the components						
Glass sample	TeO_2	Nb_2O_5	LiO_2	CaO	TbF_3	Sm_2O_3	Yb_2O_3
TNLC-0.5Tb	60	18	12	9.5	0.5	0	0
TNLC-0.5Sm	60	18	12	9.5	0	0.5	0
TNLC-0.5Tb0.5Sm	60	18	12	9.0	0.5	0.5	0
TNLC-0.6Tb0.5Sm	60	18	12	8.9	0.6	0.5	0
TNLC-0.7Tb0.5Sm	60	18	12	8.8	0.7	0.5	0
TNLC-0.8Tb0.5Sm	60	18	12	8.7	0.8	0.5	0
TNLC-0.9Tb0.5Sm	60	18	12	8.6	0.9	0.5	0
TNLC-1.0Tb0.5Sm	60	18	12	8.5	1.0	0.5	0
TNLC-0.5Tb0.6Sm	60	18	12	8.9	0.5	0.6	0
TNLC-0.5Tb0.7Sm	60	18	12	8.8	0.5	0.7	0
TNLC-0.5Tb0.8Sm	60	18	12	8.7	0.5	0.8	0
TNLC-0.5Tb0.9Sm	60	18	12	8.6	0.5	0.9	0
TNLC-0.5Tb1.0Sm	60	18	12	8.5	0.5	1.0	0
TNLC-0.5Tb0.5Sm2Yb	60	18	12	7.0	0.5	0.5	2
TNLC-0.6Tb0.5Sm2Yb	60	18	12	6.9	0.6	0.5	2
TNLC-0.7Tb0.5Sm2Yb	60	18	12	6.8	0.7	0.5	2
TNLC-0.8Tb0.5Sm2Yb	60	18	12	6.7	0.8	0.5	2
TNLC-1.0Tb0.5Sm2Yb	60	18	12	6.5	1.0	0.5	2

samples. To enhance the mechanical strength and eliminate residual thermal stresses, the glass samples were annealed at approximately 342 °C for 10 hours.[26,27] The TNLC glass materials used for optical measurements were cut into samples with approximate dimensions of 10 mm × 10 mm × 2 mm. These TNLC glass samples were then thoroughly polished on the edges and surfaces. Differential thermal analysis (DTA) was performed on a Shimadzu DTG-60H TG/DTA. The absorption spectra of the TNLC glasses in the wavelength range of 350–2000 nm were recorded using a Hitachi U-4100 UV/VIS/NIR spectrophotometer. The excitation, visible, and UC emission spectra of the Tb^{3+}-doped, Sm^{3+}-doped, Tb^{3+}–Sm^{3+} co-doped, Tb^{3+}–Sm^{3+}–Yb^{3+} tri-doped TNLC glasses were measured in the wavelength range of 200 to 750 nm using an Edinburgh Instruments FLS-1000 photoluminescence spectrometer. All the absorption, excitation, visible, and UC emission spectral measurements, and decay lifetime analyses of the TNLC glass samples were performed at ambient temperature.[26,27]

3. Results and discussion

DTA was conducted to investigate the thermal stability and glass-forming ability of the lithium–niobium–tellurite glass using the TNLC-0.5Tb0.5Sm2Yb glass sample. The DTA curve was recorded in the 100 to 1000 °C temperature range at a constant heating rate (typically 10 °C min^{-1}) under a nitrogen atmosphere. The DTA curve revealed typical thermal parameters. The onset of endothermic deviation in the DTA curve corresponded with the glass transition temperature (T_g), which was observed at approximately 342 °C. This T_g value indicates the temperature at which the amorphous glass matrix transitions from a rigid, glassy state to a more flexible, rubbery state. A relatively low T_g is characteristic of tellurite-based glasses and is attributed to the weak Te–O bonds and the open network structure of the tellurite matrix. An exothermic peak was observed at around 493 °C, corresponding to the onset of crystallization (T_x). This temperature indicates the initiation of structural reorganization and phase separation within the glass matrix, leading to the formation of crystalline phases.[16,28,29] The difference between T_x and T_g was $\Delta T = T_x - T_g = (493 - 342)$°C = 151 °C; often referred to as the thermal stability window, it is an important parameter to evaluate glass stability against devitrification.[16,29,30] For the TNLC-0.5Tb0.5Sm2Yb sample, the ΔT of approximately 151 °C indicates reasonably good thermal stability and suggests that the material is suitable for optical applications that require thermal processing.[16] Besides, the values of crystallization temperature (T_c) and crystallization peak temperatures T_p (including T_{p1}, T_{p2}, and T_{p3} temperatures)[16] were also determined to be ~598, 637, 786, and 851 °C, respectively, as depicted in Fig. 1.

The absorption spectra of TNLC-0.5Tb, TNLC-0.5Sm, TNLC-0.5Tb0.5Sm, and TNLC-0.5Tb0.5Sm2Yb lithium–niobium–tellurite glass samples are shown in Fig. 2. The absorption spectra characterize the Tb^{3+} ions due to f–f transitions. These transitions typically occur in the ultraviolet (UV) and visible wavelength regions, primarily at ~398 and 480 nm, corresponding to the $^7F_6 \rightarrow {}^5D_3$ and $^7F_6 \rightarrow {}^5D_4$ transitions of Tb^{3+} ions.[18,31] Sm^{3+} has different absorption characteristics from Tb^{3+}, primarily because of the 4f states. The absorption peaks of Sm^{3+} are typically broader than those of the Tb^{3+} ions due to the nature of its electronic transitions. The absorption spectrum of Sm^{3+} in the wavelength range of 350–2000 nm includes peaks at ~360, 374, 402, 473, 939, 1076, 1224, 1369, 1472, and 1536 nm attributed to the $^6H_{5/2} \rightarrow {}^6P_{7/2}$, $^4F_{5/2}$, $^4F_{7/2}$, $^4I_{11/2}$, $^6F_{11/2}$, $^6F_{9/2}$, $^6F_{7/2}$, $^6F_{5/2}$, $^6F_{3/2}$ and $^6H_{15/2}$ transitions, respectively.[4,22,32] The absorption spectrum of the Tb^{3+}–Sm^{3+} co-doped TNLC-0.5Tb0.5Sm glass sample in the wavelength range of 350–2000 nm contains all the absorption peaks of Tb^{3+} and Sm^{3+} ions.[4,22,32–34] The absorption spectrum of the Tb^{3+}–Sm^{3+}–Yb^{3+} tri-doped TNLC-0.5Tb0.5Sm2Yb glass sample in the wavelength range of 350–2000 nm includes all the absorption peaks of Tb^{3+}, Sm^{3+} ions and the absorption peak of Yb^{3+} ions at ~975 nm ($^2F_{7/2} \rightarrow {}^2F_{5/2}$).

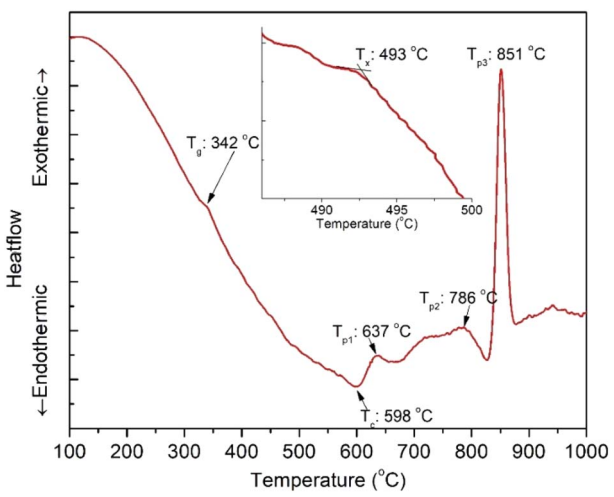

Fig. 1 DTA analysis of the TNLC-0.5Tb0.5Sm2Yb lithium–niobium–tellurite glass sample.

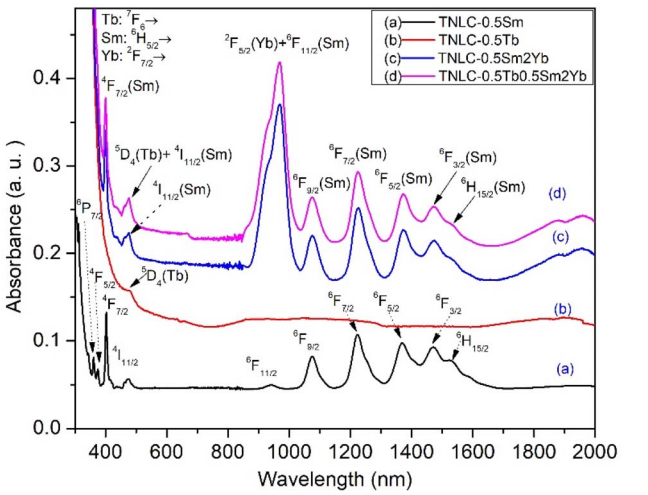

Fig. 2 Absorption spectra of TNLC-0.5Tb, TNLC-0.5Sm, TNLC-0.5Tb0.5Sm, and TNLC-0.5Tb0.5Sm2Yb lithium–niobium–tellurite glass samples.

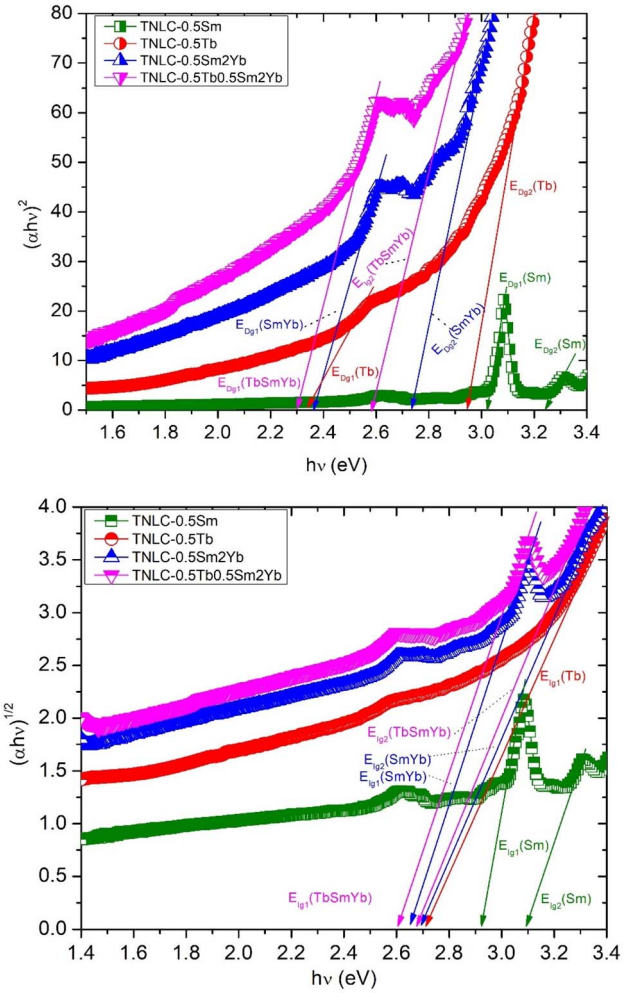

Fig. 3 (a) Direct optical bandgaps of the TNLC-0.5Sm, TNLC-0.5Tb, TNLC-0.5Sm2Yb, and TNLC-0.5Tb0.5Sm2Yb glass samples. (b) Indirect optical bandgaps of the TNLC-0.5Sm, TNLC-0.5Tb, TNLC-0.5Sm2Yb, and TNLC-0.5Tb0.5Sm2Yb glass samples.

The direct optical bandgaps (DOB) and indirect optical bandgaps (IOB) of the TNLC-0.5Sm, TNLC-0.5Tb, TNLC-0.5Sm2Yb, and TNLC-0.5Tb0.5Sm2Yb glass samples were calculated and analyzed based on their absorption spectra using the Tauc formula:[19,35,36]

$$\alpha(\lambda) = B\frac{(h\nu - E_g)^{\gamma}}{h\nu} \quad (1)$$

Here, $\alpha(\lambda)$ is the absorption coefficient; λ is the wavelength; ν is the frequency; h is the Planck constant; B is the energy-independent constant;[19,35,36] E_g is the energy gap of the glass samples; $\gamma = 2$ for DOB; $\gamma = \frac{1}{2}$ for IOB.[19,35,36] The calculated direct optical bandgaps (DOB) of the TNLC-0.5Sm, TNLC-0.5Tb, TNLC-0.5Sm2Yb, and TNLC-0.5Tb0.5Sm2Yb glass samples are shown in Fig. 3(a).

Similarly, the indirect optical bandgaps of the TNLC-0.5Sm, TNLC-0.5Tb, TNLC-0.5Sm2Yb, and TNLC-0.5Tb0.5Sm2Yb glass samples were calculated based on their absorption spectra using the Tauc formula, as shown in Fig. 3(b). A summary of the energy indirect/direct bandgap values of the TNLC-0.5Tb, TNLC-0.5Sm, TNLC-0.5Tb0.5Sm, and TNLC-0.5Tb0.5Sm2Yb glass samples is presented in Table 2.

As shown in Table 2, all the glass samples exhibited significantly smaller bandgaps than pure TeO_2 glass. The incorporation of Nb_2O_5, CaO, and Li_2O introduces electronic states within the TeO_2 bandgap, resulting in a notable reduction in the band gap. Among the samples, the TNLC-0.5Sm glass sample had a larger bandgap than the TNLC-0.5Tb glass sample, though both remain smaller than that of pure TeO_2. This reduction is attributed to the addition of RE ions, which alter the glass network by modifying oxygen bonding, increasing non-bridging oxygen content, and affecting light absorption. Furthermore, the TNLC-0.5Sm2Yb and TNLC-0.5Tb0.5Sm2Yb glass samples showed even lower bandgaps owing to the higher RE ion concentrations, which introduced additional intermediate energy levels and further enhanced non-bridging oxygen states. The increasing concentration of RE ions in the glass matrix also increases the non-bridging oxygen bonding state, causing the band gap of the glass to decrease.

The excitation spectra of the TNLC-0.5Tb, TNLC-0.5Sm, and TNLC-0.5Tb0.5Sm glass samples were obtained, as shown in Fig. 4, to determine the excitation wavelengths for the TNLC glass samples containing both Tb^{3+} and Sm^{3+} ions. Based on the spectral data, we chose 374 nm as the excitation wavelength for the Tb^{3+}-Sm^{3+} co-doped TNLC glass sample.[37,38]

The visible emission spectra of the TNLC-0.5Tb, TNLC-0.5Sm, and TNLC-0.5Tb0.5Sm lithium–niobium–tellurite glass samples under 374 nm are shown in Fig. 5. For the TNLC-0.5Tb glass sample, the visible emission of Tb^{3+} under 374 nm excitation revealed weaker peaks at around 415 and 438 nm due to the $^3D_5 \rightarrow {}^7F_5$ and $^3D_5 \rightarrow {}^7F_4$ transitions.[4,16,32] This result is intriguing because these emission peaks have not been reported in most previous works. For the TNLC-0.5Sm glass sample, the

Table 2 Indirect/direct energy bandgap values of the TNLC-0.5Tb, TNLC-0.5Sm, TNLC-0.5Tb0.5Sm, and TNLC-0.5Tb0.5Sm2Yb glass samples

	Direct bandgap values			Indirect bandgap values		
Glass sample	E_{Dg1} (eV)	E_{Dg2} (eV)	$\Delta E_D = E_{Dg2} - E_{Dg1}$ (eV)	E_{Ig1} (eV)	E_{Ig2} (eV)	$\Delta E_I = E_{Ig2} - E_{Ig1}$ (eV)
TNLC-0.5Sm	3.02	3.23	0.21	2.98	3.19	0.21
TNLC-0.5Tb	2.34	2.95	0.61	2.84	—	—
TNLC-0.5Sm2Yb	2.36	2.74	0.38	2.75	2.82	0.07
TNLC-0.5Tb0.5Sm2Yb	2.28	2.59	0.31	2.72	2.79	0.07

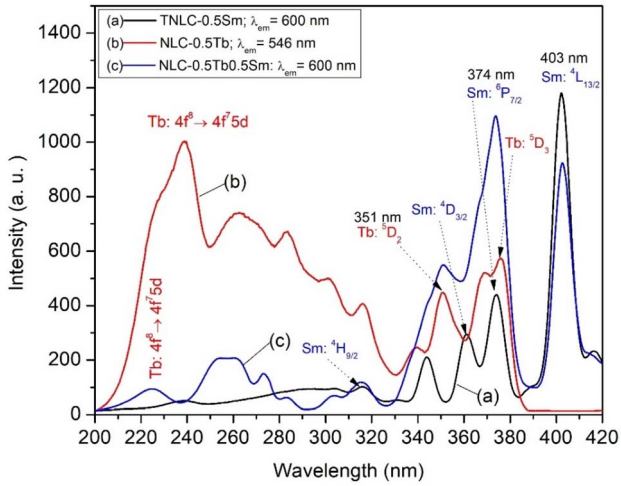

Fig. 4 Excitation spectra of the TNLC-0.5Tb, TNLC-0.5Sm, and TNLC-0.5Tb0.5Sm lithium–niobium–tellurite glass samples.

visible emission peaks of Sm^{3+} under 374 nm excitation at around 440, 564, 601, and 645 nm could be attributed to the $^4G_{7/2} \rightarrow {}^6H_{9/2}$, $^4G_{5/2} \rightarrow {}^6H_{5/2}$, $^4G_{5/2} \rightarrow {}^6H_{7/2}$, and $^4G_{5/2} \rightarrow {}^6H_{9/2}$ transitions, respectively.[32–34] For the TNLC-0.5Tb0.5Sm glass sample, the visible emission of peaks co-doped Tb^{3+} and Sm^{3+} under 374 nm excitation were found at around 415, 438, 490, 546, 587, 622, and 645 nm due to transitions from Tb^{3+}, Sm^{3+} ions or the combination of transitions from both Tb^{3+} and Sm^{3+} ions corresponding to (Tb^{3+}: $^5D_5 \rightarrow {}^7F_5$), ($Tb^{3+}$: $^5D_5 \rightarrow {}^7F_4$ + Sm^{3+}: $^4G_{7/2} \rightarrow {}^6H_{9/2}$), ($Tb^{3+}$: $^5D_4 \rightarrow {}^7F_{J(=6,\ 5,\ 4,\ \text{and}\ 3)}$) and ($Sm^{3+}$: $^4G_{5/2} \rightarrow {}^6H_{9/2}$) transitions, respectively.[4,32–34]

The Commission Internationale de L'Eclairage (CIE) 1931 (x; y) chromaticity coordinates[19,39] for the visible emission spectra of the TNLC-0.5Tb, TNLC-0.5Sm, and TNLC-0.5Tb0.5Sm glass samples were determined to be P_{Tb} (0.2840; 0.5303), $P_{Tb–Sm}$ (0.2901; 0.3728), and P_{Sm} (0.4906; 0.3537) located in the yellow-pink, yellowish-green and black body curve regions, respectively, as shown in Fig. 6.

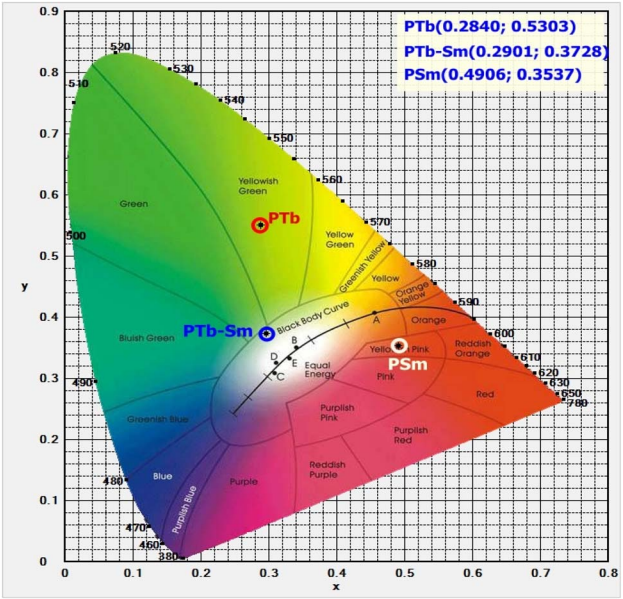

Fig. 6 CIE 1931 (x; y) color coordinates for the visible emission spectra of the TNLC-0.5Tb, TNLC-0.5Sm, and TNLC-0.5Tb0.5Sm glass samples under 374 nm excitation.

The visible emission spectra of the TNLC-pTb0.5Sm (p = 0.6, 0.7, 0.8, 0.9, and 1.0 mol%) lithium–niobium–tellurite glass samples under 374 nm are shown in Fig. 7. With the increase in molar concentration of Tb^{3+} from 0.6 to 1.0 mol%, the visible emission intensity of the peaks of Tb^{3+} ions at ~415, 438, 490, 546, and 622 nm increased significantly.[32,33] Similarly, the visible emission intensity of the Sm^{3+} ion peaks at around 645 nm, which is attributed to the $^4G_{5/2} \rightarrow {}^6H_{9/2}$ transition, was also increased. These findings confirm that energy from the neighboring states of Tb^{3+} ions were transferred to the $^4G_{5/2} \rightarrow {}^6H_{9/2}$ transition of Sm^{3+} ions.[33,34,37–40]

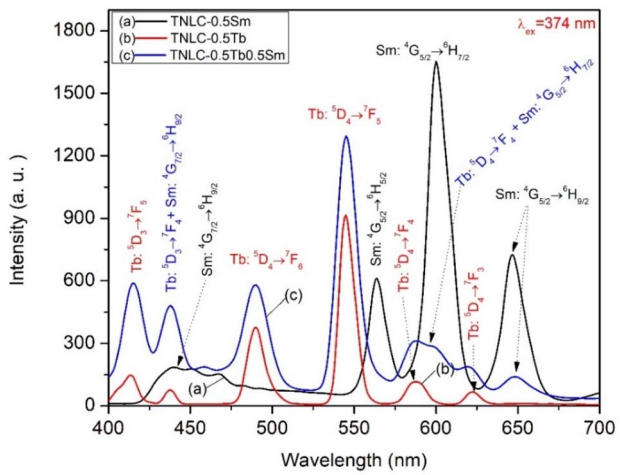

Fig. 5 Visible emission spectra of the TNLC-0.5Tb, TNLC-0.5Sm, and TNLC-0.5Tb0.5Sm lithium–niobium–tellurite glass samples under 374 nm excitation.

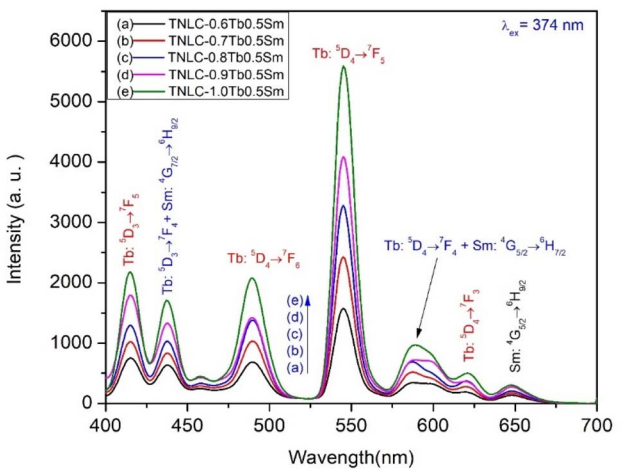

Fig. 7 Visible emission spectra of the TNLC-pTb0.5Sm (p = 0.6, 0.7, 0.8, 0.9, and 1.0 mol%) glass samples under 374 nm excitation.

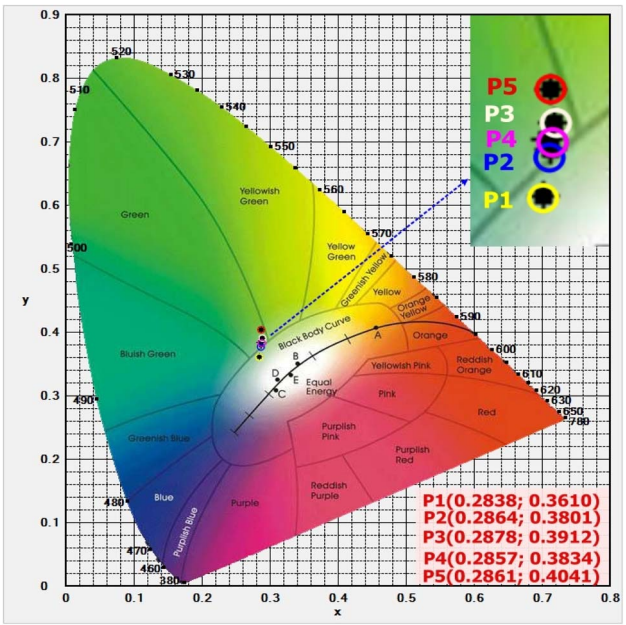

Fig. 8 CIE 1931 (x; y) color coordinates for the visible emission spectra of the TNLC-pTb0.5Sm (p = 0.6, 0.7, 0.8, 0.9, and 1.0 mol%) glass samples under 374 nm excitation.

Fig. 8 shows the CIE1931 (x; y) color coordinates for the visible emission spectra of the TNLC-pTb0.5Sm (p = 0.6, 0.7, 0.8, 0.9, and 1.0 mol%) lithium–niobium–tellurite glass samples under excitation at 374 nm. With the increase in the molar concentration of Tb^{3+} ions from 0.6 to 1.0 mol%, the color points of the visible emission spectra of the Tb^{3+}–Sm^{3+} co-doped glass shifted in the order of P1 (0.2838; 0.3610), P2 (0.2864; 0.3801), P3 (0.2878; 0.3912), P4 (0.2857; 0.3834) and P5 (0.2861; 0.4041) in the CIE1931 (x; y) color coordinate chart, respectively,[19,33,34] as shown in Fig. 8. From the results in Fig. 8, we can see that the TNLC-0.6Tb0.5Sm sample corresponding to the Tb^{3+}/Sm^{3+} concentration ratio of 1.2 has the color point closest to the white light region.[33,34]

To further investigate the optimal concentration ratio between Tb^{3+} and Sm^{3+} ions for the color point to move closer to the white light region, which is necessary for application to WLEDs, the Sm^{3+} concentration was changed while keeping the Tb^{3+} concentration constant to investigate the emission of the Tb^{3+}–Sm^{3+} co-doped glass sample. The visible emission spectra of the TNLC-0.5TbqSm (q = 0.6, 0.7, 0.8, 0.9, and 1.0 mol%) lithium–niobium–tellurite glass samples under 374 nm are shown in Fig. 9.

When excited at 374 nm, with an increase in Sm^{3+} concentration from 0.6 to 1.0 mol%, most of the emission peaks of both Sm^{3+} and Tb^{3+} ions increased in intensity. This result affirms that energy from the neighboring states of Sm^{3+} ions is transferred to the Tb^{3+} ions. Simultaneously, with the increase in molar concentration of Sm^{3+} ions from 0.6 to 1.0 mol%, the tunable color for the visible emission spectra of the Tb^{3+}–Sm^{3+} co-doped glass samples shifted to color points 1 (0.3118; 0.3821), 2 (0.3093; 0.3827), 3 (0.3095; 0.3875), 4 (0.3169; 0.3937) and 5 (0.3263; 0.4049) on the CIE 1931 (x; y) coordinate

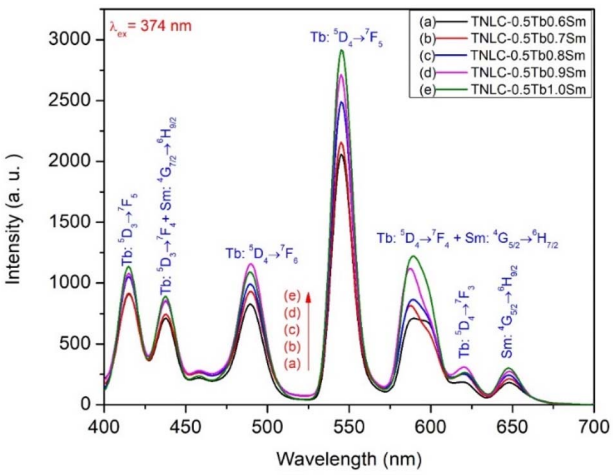

Fig. 9 Visible emission spectra of the TNLC-0.5TbqSm (q = 0.6, 0.7, 0.8, 0.9, and 1.0 mol%) glass samples under 374 nm excitation.

diagram,[19,33,34] as shown in Fig. 10. From the visible emission spectra results of the Tb^{3+}–Sm^{3+} co-doped glass samples under 374 nm excitation (Fig. 7 and 9), as well as the color coordinates for their visible emission spectra (Fig. 8 and 10), we determined the optimal concentration ratio of Tb^{3+} and Sm^{3+} ions to be 0.83 for the color point to move the closest to the white light region, corresponding to the TNLC-0.5Tb0.6Sm glass sample.

During the analysis of the absorption capacity of the materials in the infrared region, we observed that the material strongly absorbed in the range from 940 to 1070 nm, with a maximum peak at about 980 nm. We surveyed the UC emission process of the Tb^{3+}–Sm^{3+}–Yb^{3+} co-doped material samples to investigate the ET process between Yb^{3+} ions and Tb^{3+}/Sm^{3+}

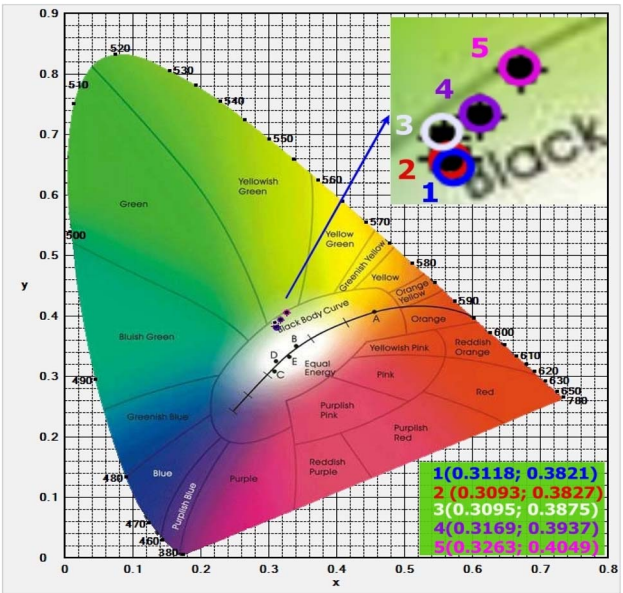

Fig. 10 CIE1931 (x; y) color coordinates for the visible emission spectra of the TNLC-0.5TbqSm (q = 0.6, 0.7, 0.8, 0.9, and 1.0 mol%) glass samples under 374 nm excitation.

ions. In addition to investigating the VIS emission spectra of Tb^{3+}–Sm^{3+} co-doped glass samples, we conducted further investigations using the UC emission spectra of these samples. Fig. 11 shows the UC emission spectra of the TNLC-*p*Tb0.5Sm2Yb (p = 0.5, 0.6, 0.7, 0.8, and 1.0 mol%) lithium–niobium–tellurite glass samples under a 980 nm laser diode (LD). With the increase in molar concentration of Tb^{3+} from 0.5 to 1.0 mol%, the UC emission intensity of the Tb^{3+} ion peaks at around 415, 438, 490, 546, and 622 nm increased for the Tb^{3+}–Sm^{3+}–Yb^{3+} co-doped glass samples.[41] Meanwhile, the UC emission intensity of the peaks at around 645 nm, attributed to the $^4G_{5/2} \rightarrow {}^6H_{9/2}$ transition of Sm^{3+} ions, was also increased. This result confirms that energy from the neighboring states of Tb^{3+} ions was transferred to the $^4G_{5/2} \rightarrow {}^6H_{9/2}$ transition of Sm^{3+} ions.[39,40]

Fig. 12 shows the CIE 1931 (x; y) color coordinates for the UC emission spectra of the TNLC-*p*Tb0.5Sm (p = 0.5, 0.6, 0.7, 0.8, and 1.0 mol%) lithium–niobium–tellurite glass samples under a 980 nm LD. With the increase in molar concentration of Tb^{3+} ions from 0.5 to 1.0 mol%, the color points shifted from in the order of points A (0.3277; 0.4847), B (0.2974; 0.5169), C (0.2997; 0.5441), D (0.3050; 0.5676), and E (0.3167; 0.5782) on the CIE 1931 (x; y) color coordinate diagram and were mainly located in the yellowish-green region.

To further determine the roles of excitation wavelength and the molar concentration of the doped RE ions on the CIE 1931 (x; y) color coordinates and color region, we compared the results obtained in this study with previously published reports, as listed in Table 3.

Investigation and calculation of correlated color temperature (CCT) are essential for optimizing the output light quality. From the CIE 1931 (x; y) results, the CCT of the TNLC glass samples was calculated using the McCamy formula (often called McCamy's approximation):[50,52]

$$\mathrm{CCT} = an^3 + bn^2 + cn + d \approx -449n^3 + 3525n^2 - 6823.3n + 5520.33 \quad (3)$$

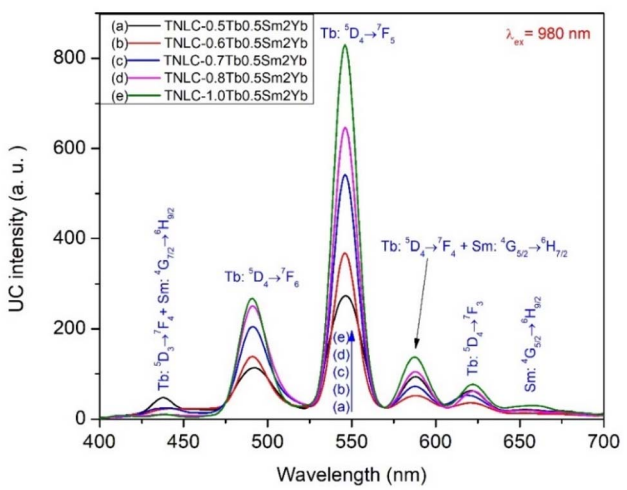

Fig. 11 UC emission spectra of the TNLC-*p*Tb0.5Sm2Yb (p = 0.5, 0.6, 0.7, 0.8, and 1.0 mol%) glass samples under 980 nm LD excitation.

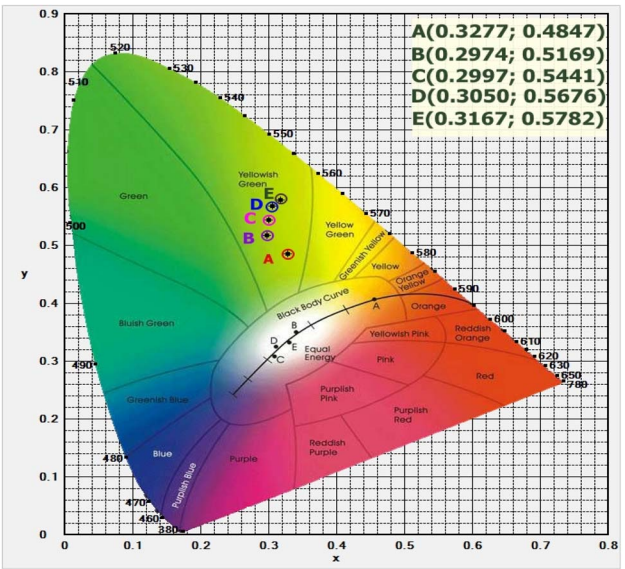

Fig. 12 CIE 1931 (x; y) color coordinates for the UC emission spectra of the TNLC-*p*Tb0.5Sm2Yb (p = 0.5, 0.6, 0.7, 0.8, and 1.0 mol%) glass samples excited under a 980 nm LD.

where:

$$n = \frac{x - x_e}{y - y_e}, \quad (4)$$

Here, x and y are the CIE 1931 (x; y) chromaticity coordinates of the light source; x_e = 0.3320 and y_e = 0.1858 are the chromaticity coordinates of the Planckian locus.[50,52] The CCT calculation results of the as-prepared glass samples are described in detail in Table 4.

The energy level diagram of the visible and UC emissions corresponding to the transitions of the Tb^{3+}–Sm^{3+} and Tb^{3+}–Sm^{3+}–Yb^{3+} co-doped glass materials under excitation wavelengths of 374 nm and 980 nm is shown in Fig. 13. The Tb^{3+} ions are excited from the ground state $^3H_6$ to the higher-energy state $^3D_5$. These ions show characteristic emission in the visible region due to $^3D_{5 \text{ and } 4} \rightarrow {}^5F_{J\ (J = 3, 4, 5, \text{and } 6)}$ transitions.[39] Under 374 nm excitation, the visible emission of Tb^{3+} peaks at around 490, 546, 587, and 622 nm, which can be attributed to the $^3D_4 \rightarrow {}^5F_{J\ (J = 6, 5, 4, \text{and } 3)}$ transitions. The Sm^{3+} ions, when excited at 374 nm, move from the $^6H_{5/2}$ ground state to a higher-energy $^6P_{7/2}$ state.[40] From this $^6P_{7/2}$ state, energy is transferred to $^4G_{5/2}$ lower-energy states through non-radiative and ET processes. The ET1, ET2, CET1, and CET2 processes shown in Fig. 13 can be described in detail as follows:[41,51,53]

$$\mathrm{ET1}: {}^5D_4(Tb^{3+}) + {}^4G_{7/2}(Sm^{3+}) \rightarrow {}^5F_6(Tb^{3+}) + {}^6H_{5/2}(Sm^{3+}).$$

$$\mathrm{ET2}: {}^4G_{5/2}(Sm^{3+}) + {}^5D_4(Tb^{3+}) \rightarrow {}^6H_{7/2}(Sm^{3+}) + {}^7F_6(Tb^{3+}).$$

$$\mathrm{CET1}: 2^2F_{5/2}(Yb^{3+}) + {}^7F_6(Tb^{3+}) \rightarrow 2^2F_{7/2}(Yb^{3+}) + {}^5D_4(Tb^{3+}).$$

$$\mathrm{CET2}: 2^2F_{5/2}(Yb^{3+}) + {}^6H_{5/2}(Sm^{3+}) \rightarrow 2^2F_{7/2}(Yb^{3+}) + {}^4I_{11/2}(Sm^{3+}).$$

Table 3 Compare the energy transfer processes, color coordinates, and excitation wavelengths of RE ions in this study with those reported in previously published papers

Host material	RE co-doping ratio	λ_{ex} (nm)	Energy transfer	CIE 1931 coordinates (x; y)	Color region	References
Tellurite glass	$1Ce^{3+}$–$1Tb^{3+}$–$1Sm^{3+}$	350	$Ce^{3+} \rightarrow Tb^{3+}$	0.3750; 0.3245	Pure white	T. T. Hong *et al.*[42]
$LiYF_4$ single crystals	$1.24Tb^{3+}$–$1.63Sm^{3+}$–$0.25Ce^{3+}$	374	—	0.3084; 0.3612	Yellowish-green	Y. Z. Jiang *et al.*[43]
$Ba_3MgSi_2O_8$:phosphors	$0.12Tb^{3+}$–$0.05Sm^{3+}$	233	$Tb^{3+} \rightarrow Sm^{3+}$	0.555; 0.425	Orange yellow	X. K. Sun *et al.*[44]
Phosphate glasses	$0.5Sm^{3+}$–$0.1Tb^{3+}$	374	$Tb^{3+} \rightarrow Sm^{3+}$	0.541; 0.300	Reddish-orange	K. A. Kumar *et al.*[37]
	$1.0Sm^{3+}$–$0.1Tb^{3+}$			0.551; 0.312		
Zinc phosphate glasses	$0.5Sm^{3+}$–$1.0Tb^{3+}$	361	$Tb^{3+} \rightarrow Sm^{3+}$	0.448; 0.459	Greenish-yellow	A. N. Meza-Rocha *et al.*[45]
		374		0.407; 0.485	Yellow	
$CaWO_4$ nanoparticles	$0.5Sm^{3+}$–$0.5Tb^{3+}$	355	—	0.3098; 0.4033	White	N. F. Andrade Neto *et al.*[46]
	$1.0Sm^{3+}$–$1.0Tb^{3+}$	355		0.3002; 0.3997	Blue	
$Ca_2La_3(SiO_4)_3F$ phosphor	$0.15Tb^{3+}$,$0.04Sm^{3+}$	377	$Tb^{3+} \rightarrow Sm^{3+}$	0.4175; 0.5658	Yellow-green	K. Nie *et al.*[47]
	$0.15Tb^{3+}$–$0.18Sm^{3+}$	377		0.4691; 0.5160	Greenish-yellow	
$CaLa_4(SiO_4)_3O$:phosphors	$9\%Tb^{3+}$–$11\%Sm^{3+}$	377	$Tb^{3+} \rightarrow Sm^{3+}$	0.393; 0.387	Bright white	B. Yuan *et al.*[48]
$K_3Gd(PO_4)_2$ crystalline glass ceramics	$0.3\%Tb^{3+}$–$0.4\%Sm^{3+}$	376	$Tb^{3+} \rightarrow Sm^{3+}$	0.3201; 0.3297	White	Y. N. Guo *et al.*[49]
$K_2Y(WO_4)(PO_4)$ phosphors	$2\%Sm^{3+}$–$5\%Tb^{3+}$	377	$Sm^{3+} \rightarrow Tb^{3+}$	0.37; 0.57	Yellow-green	E. J. Ansari *et al.*[50]
Potassium-zinc phosphate glasses	$1.0Sm^{3+}$–$1.0Tb^{3+}$	344	$Tb^{3+} \rightarrow Sm^{3+}$	0.529; 0.447	Orange	O. Soriano-Romero *et al.*[51]
	$1.0Sm^{3+}$–$1.0Tb^{3+}$	360	$Tb^{3+} \rightarrow Sm^{3+}$	0.534; 0.442	Yellow	
	$1.0Sm^{3+}$–$1.0Tb^{3+}$	377	$Tb^{3+} \rightarrow Sm^{3+}$	0.442; 0.507	Yellow	
Lithium–niobium–tellurite glass	$0.5Tb^{3+}$–$0.6Sm^{3+}$	374	$Tb^{3+} \leftrightarrow Sm^{3+}$	0.3118; 0.3821	White (near black body curve)	This study
	$0.5Tb^{3+}$–$0.5Sm^{3+}$–$2Yb^{3+}$	980	$Yb^{3+} \rightarrow Tb^{3+}$	0.3277; 0.4847	Yellowish-green	
			$Yb^{3+} \rightarrow Sm^{3+}$			

Table 4 CCT values and CIE 1931 (x; y) chromaticity coordinates of the TNLC glass samples

Glass samples	λ_{ex}	Color point	CIE 1931 x	CIE 1931 y	CCT (K)	Color region
TNLC-0.5Tb	374 nm	P_{Tb}	0.2840	0.5303	6544	Yellowish green
TNLC-0.5Tb0.5Sm	374 nm	P_{Tb-Sm}	0.2901	0.3728	7208	White
TNLC-0.5Sm	374 nm	P_{Sm}	0.4906	0.3537	15 489	Yellowish pink
TNLC-0.6Tb0.5Sm	374 nm	P1	0.2838	0.3601	7662	Green
TNLC-0.7Tb0.5Sm	374 nm	P2	0.2864	0.3801	7294	Green
TNLC-0.8Tb0.5Sm	374 nm	P3	0.2878	0.3912	7129	Green
TNLC-0.9Tb0.5Sm	374 nm	P4	0.2857	0.3834	7290	Green
TNLC-1.0Tb0.5Sm	374 nm	P5	0.2861	0.4041	7085	Green
TNLC-0.5Tb0.6Sm	374 nm	1	0.3118	0.3821	6254	White
TNLC-0.5Tb0.7Sm	374 nm	2	0.3093	0.3827	6347	White
TNLC-0.5Tb0.8Sm	374 nm	3	0.3095	0.3875	6318	White
TNLC-0.5Tb0.9Sm	374 nm	4	0.3169	0.3937	6033	White
TNLC-0.5Tb1.0Sm	374 nm	5	0.3263	0.4049	5706	White
TNLC-0.5Tb0.5Sm2Yb	980 nm	A	0.3277	0.4847	5616	Yellowish green
TNLC-0.6Tb0.5Sm2Yb	980 nm	B	0.2974	0.5169	6274	Yellowish green
TNLC-0.7Tb0.5Sm2Yb	980 nm	C	0.2997	0.5441	6165	Yellowish green
TNLC-0.8Tb0.5Sm2Yb	980 nm	D	0.3050	0.5676	6020	Yellow
TNLC-1.0Tb0.5Sm2Yb	980 nm	E	0.3167	0.5782	5790	Yellowish green

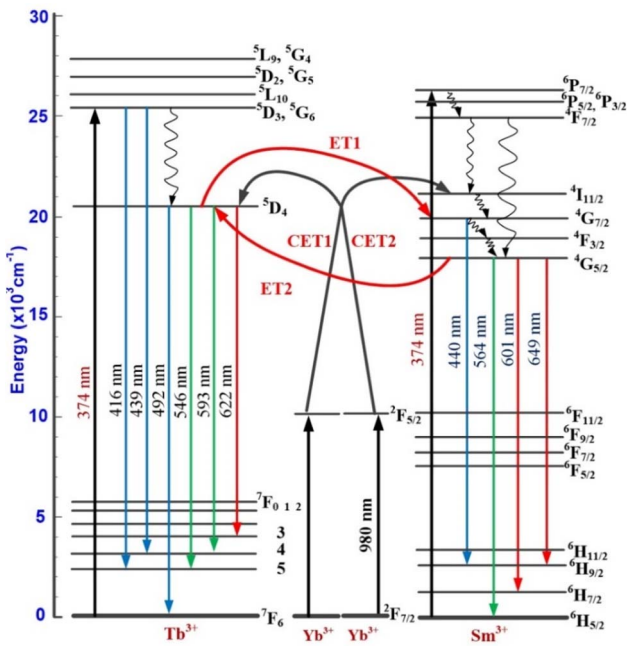

Fig. 13 Energy levels of the Tb^{3+}, Sm^{3+}, and Yb^{3+} ions and the mechanisms of visible and UC emissions *via* CET1, CET2, ET1, and ET2 processes in the TNLC glass system.

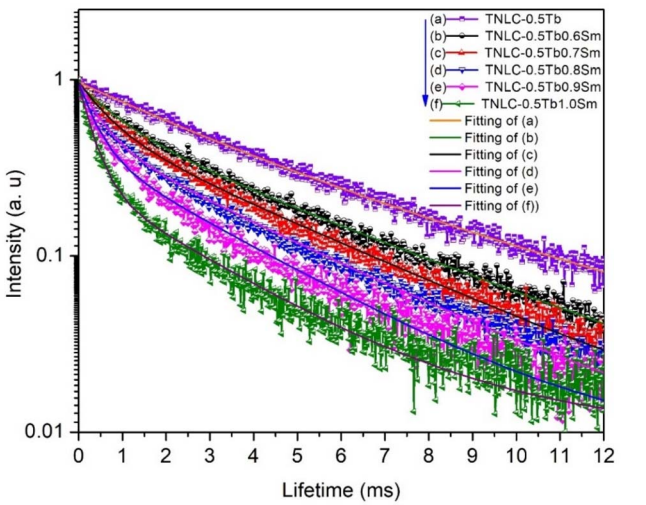

Fig. 14 Decay lifetimes of Tb^{3+} at the $^5D_4 \rightarrow {}^5F_6$ transition in TNLC-0.5TbqSm (q = 0, 0.6, 0.7, 0.8, 0.9, and 1.0 mol%) glass samples under 374 nm excitation.

The charge transfer process between the Tb^{3+} and Sm^{3+} ions depends on the concentration of optical centers in the material. To further investigate the influence of Tb^{3+} ion concentration on the ET process, we analyzed the decay lifetimes of Tb^{3+} and Sm^{3+} ions in the synthesized TNLC glass materials. We measured the time-resolved fluorescence spectra of TNLC-0.5TbqSm (q = 0, 0.6, 0.7, 0.8, 0.9, and 1.0 mol%) lithium–niobium–tellurite glass samples using an excitation wavelength of 374 nm and emission at 546 nm corresponding to the $^5D_4 \rightarrow {}^5F_6$ transition of Tb^{3+};[4,32–34] the obtained results are presented in Fig. 14. Through the fitting process, we observed that the time-resolved fluorescence spectra of the materials followed the equation:[16,50]

$$I_t = A_1 \exp\left(-\frac{t}{\tau_1}\right) + A_2 \exp\left(-\frac{t}{\tau_2}\right), \quad (5)$$

where τ_1 and τ_2 are the decay lifetime components, and A_1 and A_2 are constants. The average decay lifetime τ was calculated as follows:[16,51,54,55]

$$\tau = \frac{A_1\tau_1^2 + A_2\tau_2^2}{A_1\tau_1 + A_2\tau_2}. \quad (6)$$

The decay lifetimes of TNLC-0.5TbqSm (q = 0, 0.6, 0.7, 0.8, 0.9, and 1.0 mol%) lithium–niobium–tellurite glass samples

Table 5 Decay lifetimes of Tb^{3+} ions at 546 nm ($^5D_4 \rightarrow {}^5F_6$) and Sm^{3+} ions at 564 nm ($^4G_{5/2} \rightarrow {}^6H_{5/2}$) under 374 nm excitation

Glass sample	Decay lifetime (ms)
TNLC-0.5Tb	4.62
TNLC-0.5Tb0.6Sm	3.97
TNLC-0.5Tb0.7Sm	3.48
TNLC-0.5Tb0.8Sm	3.13
TNLC-0.5Tb0.9Sm	2.63
TNLC-0.5Tb1.0Sm	2.21
TNLC-0.5Sm	7.86
TNLC-0.6Tb0.5Sm	6.91
TNLC-0.7Tb0.5Sm	5.63
TNLC-0.8Tb0.5Sm	4.24
TNLC-0.9Tb0.5Sm	3.18
TNLC-1.0Tb0.5Sm	2.56

calculated according to formula (6) are listed in Table 5. The decay lifetimes at 546 nm, corresponding to the $^5D_4 \rightarrow {}^5F_6$ transition of Tb^{3+} ions in the TNLC-0.5Tb*q*Sm (q = 0, 0.6, 0.7, 0.8, 0.9, and 1.0 mol%) lithium–niobium–tellurite glass samples, were found to decrease with increasing Sm^{3+} concentration. This is strong evidence for ET from Tb^{3+} to Sm^{3+} ions.[4,32–34,44] Similarly, the decay lifetimes of Sm^{3+} ions at 601 nm, corresponding to the $^4G_{5/2} \rightarrow {}^6H_{7/2}$ transition of Sm^{3+} ions[4,32–34] in the TNLC-*p*Tb0.5Sm (p = 0, 0.6, 0.7, 0.8, 0.9, and 1.0 mol%) lithium–niobium–tellurite glass samples, were measured under 374 nm excitation, as shown in Fig. 15. The average decay lifetimes of TNLC-*p*Tb0.5Sm (p = 0, 0.6, 0.7, 0.8, 0.9, and 1.0 mol%) lithium–niobium–tellurite glass samples were calculated, as presented in Table 5. The decay lifetimes of Sm^{3+} at 601 nm, corresponding to $^4G_{5/2} \rightarrow {}^6H_{7/2}$ transition of Sm^{3+} ions[32,33] in these glass samples under 374 nm excitation were found to decrease with increasing Tb^{3+} concentration in the glass samples, further proving ET from Sm^{3+} to Tb^{3+} ions.[33,34,39,40]

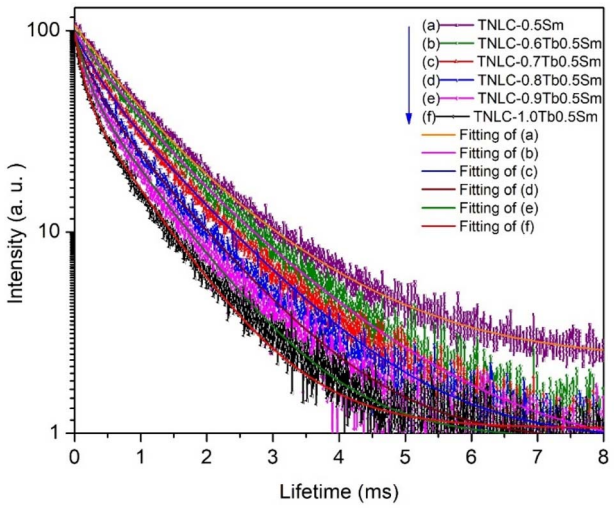

Fig. 15 Decay lifetimes of Sm^{3+} at the $^4G_{5/2} \rightarrow {}^6H_{5/2}$ transition in TNLC-*p*Tb0.5Sm (p = 0, 0.6, 0.7, 0.8, 0.9, and 1.0 mol%) glass samples under 374 nm excitation.

To evaluate the energy transfer efficiency (ETE) between Tb^{3+} and Sm^{3+} ions, we carried out ETE calculations for these ET processes. The ETE from Tb^{3+} to Sm^{3+} ions is denoted as $\eta_{ET(Tb \rightarrow Sm)}$ and was estimated using the luminescence lifetimes of the donor (Tb^{3+}) in the presence and absence of the acceptor (Sm^{3+}), according to the following equation:

$$\eta_{ET(Tb \rightarrow Sm)} = 1 - \frac{\tau_{Tb-Sm}}{\tau_{Tb}}, \quad (7)$$

where τ_{Tb} is the luminescence lifetime of Tb^{3+} ions in the absence of Sm^{3+} ions, and τ_{Tb-Sm} is the luminescence lifetime of Tb^{3+} ions in the presence of Sm^{3+} ions (*i.e.* when energy transfer occurs).

Similarly, the ETE from Sm^{3+} to Tb^{3+} ions is denoted as $\eta_{ET(Sm \rightarrow Tb)}$ and was estimated using the luminescence lifetimes of the donor (Sm^{3+}) in the presence and absence of the acceptor (Tb^{3+}), according to the following equation:

$$\eta_{ET(Sm \rightarrow Tb)} = 1 - \frac{\tau_{Sm-Tb}}{\tau_{Sm}}, \quad (8)$$

where τ_{Sm} is the luminescence lifetime of Sm^{3+} ions in the absence of Tb^{3+} ions, and τ_{Sm-Tb} is the luminescence lifetime of Sm^{3+} ions in the presence of Tb^{3+} ions. Based on the results presented in Table 5, we calculated ETE values to be 52.26% and 67.43% for the ET processes from Tb^{3+} to Sm^{3+} ions and from Sm^{3+} to Tb^{3+} ions, respectively.

4. Conclusions

In this study, a series of Tb^{3+}-doped, Sm^{3+}-doped, Tb^{3+}-Sm^{3+} co-doped, and Tb^{3+}–Sm^{3+}–Yb^{3+} tri-doped lithium–niobium–tellurite TeO_2–Nb_2O_5–LiO_2–CaO glasses were synthesized *via* conventional melt-quenching. These glasses exhibited tunable multi-color emissions under excitation at 374 nm and 980 nm, which could be attributed to Sm^{3+} (yellow-pink), Tb^{3+} (yellowish-green), and Yb^{3+}-sensitized UC emissions of Tb^{3+}–Sm^{3+}–Yb^{3+} tri-doped glass materials. The DTA analysis showed the high thermal stability of the tri-doped glass, with $\Delta T = 151$ °C, suitable for heat treatment and mechanical durability. The emission color could be effectively controlled by varying the Sm^{3+}–Tb^{3+} concentrations and excitation wavelengths. The optimal Tb^{3+}/Sm^{3+} molar ratio was 0.83 in the TNLC-0.5Tb0.6Sm sample for achieving CIE coordinates closest to white light emission. Spectral and lifetime measurements confirmed ETE between Tb^{3+} and Sm^{3+} ions. The combination of low phonon energy, high stability, emission tunability, and efficient ET highlights the potential of Tb^{3+}–Sm^{3+} co-doped and Tb^{3+}–Sm^{3+}–Yb^{3+} tri-doped TNLC glasses for application in advanced color display and solid-state lighting devices, including WLEDs.

Data availability

The authors confirm that the data supporting the findings of this study are available from the corresponding author upon request.

Conflicts of interest

There are no conflicts of interest to declare.

Acknowledgements

The corresponding author (Ho Kim Dan) would like to express his gratitude to Van Lang University.

References

1 G. J. Li, M.-C. Tseng, Y. Chen, F. S.-Y. Yeung, H. Y. He, Y. C. Cheng, J. H. Cai and E. G. Chen, Color-conversion displays: current status and future outlook, *Light:Sci. Appl.*, 2024, **13**, 301, DOI: 10.1038/s41377-024-01618-8.

2 J. C. Chen, Q. L. Zhao, B. H. Yu and U. Lemmer, A review on quantum dot-based color conversion layers for mini/micro-LED displays: Packaging, light management, and pixelation, *Adv. Opt. Mater.*, 2024, **12**, 2300873, DOI: 10.1002/adom.202300873.

3 M. Vasilopoulou, A. R. B. M. Yusoff, M. Daboczi, J. Conforto, A. E. X. Gavim, W. J. D. Silva, A. G. Macedo, A. Soultati, G. Pistolis, F. K. Schneider, Y. F. Dong, P. Jacoutot, G. Rotas and J. Jang, High efficiency blue organic light-emitting diodes with below-bandgap electroluminescence, *Nat. Commun.*, 2021, **12**, 4868, DOI: 10.1038/s41467-021-25135-z.

4 T. Q. Sheng, Z. L. Fu, X. J. Wang, S. H. Zhou, S. Y. Zhang and Z. W. Dai, Solvothermal synthesis and luminescence properties of $BaCeF_5$, and $BaCeF_5$: Tb^{3+}, Sm^{3+} Nanocrystals: An approach for white light emission, *J. Phys. Chem. C*, 2012, **36**(116), 19597–19603, DOI: 10.1021/jp306935k.

5 J. S. Alzahrani, Z. A. Alrowaili, A. V. Lebedev, I. O. Olarinoye, A. Hammoud, L. V. Vasileva and M. S. Al-Buriahi, Optical properties and radiation shielding performance of tellurite glassy composites: role of rare earth oxides, *Radiat. Phys. Chem.*, 2023, **212**, 111168, DOI: 10.1016/j.radphyschem.2023.111168.

6 J. E. Stanworth, Tellurite glasses, *Nature*, 1952, **169**, 581–582, DOI: 10.1038/169581b0.

7 R. El-Mallawany, The optical properties of tellurite glasses, *J. Appl. Phys.*, 1992, **72**, 1774–1777, DOI: 10.1063/1.351649.

8 J. Lousteau, D. Milanese, S. Abrate, N. Boetti, M. Pittarelli, S. Barbero and M. Ferrari, Exploring the influence of ZnF_2 on zinc-tellurite glass: unveiling changes in OH content, structure, and optical properties, *ACS Omega*, 2023, **8**(38), 35266–35274, DOI: 10.1021/acsomega.3c05010.

9 J. Biswas, S. Jana and S. Ghosh, Investigation on luminescence characteristics of Dy^{3+}–Tb^{3+} co-doped phospho-tellurite glasses for tunable green/white LED applications, *Spectrochim. Acta, Part A*, 2025, **331**, 125756, DOI: 10.1016/j.saa.2025.125756.

10 V. K. Rai, S. B. Rai and D. K. Rai, Optical properties of Tb^{3+} doped tellurite glass, *J. Mater. Sci.*, 2004, **39**, 4971–4975, DOI: 10.1023/B:JMSC.0000035348.82074.0a.

11 K. S. Rudramamba, S. K. Taherunnisa, D. V. K. Reddy, N. Veeraiah and M. R. Reddy, The structural and warm light emission properties of Sm^{3+}/Tb^{3+} doubly doped strontium bismuth borosilicate glasses for LED applications, *Spectrochim. Acta, Part A*, 2019, **220**, 117097, DOI: 10.1016/j.saa.2019.05.002.

12 M. Vijayakumar and K. Marimuthu, Effect of Tb^{3+} concentration on Sm^{3+} doped leadfluoro-borophosphate glasses for WLED applications, *J. Non-Cryst. Solids*, 2016, **447**, 45–54, DOI: 10.1016/j.jnoncrysol.2016.05.028.

13 G. Lakshminarayana, A. N. Meza-Rocha, O. Soriano-Romero, E. F. Huerta, U. Caldiño, A. Lira, D.-E. Lee, J. H. Yoon and T. J. Park, Analysis of fluorescence characteristics of Sm^{3+}-doped B_2O_3-rich glasses for Orange-light-emitting diodes, *J. Alloys Compd.*, 2021, **884**, 161076, DOI: 10.1016/j.jallcom.2021.161076.

14 A. U. Trápala-Ramírez, J. L. N. Gálvez-Sandoval, A. Lira, I. Camarillo, E. Alvarez-Ramos, A. N. Meza-Rocha and U. Caldiño, Calcium-zinc phosphate glasses activated with Tb^{3+}/Eu^{3+} for laser and white LED applications, *J. Lumin.*, 2019, **215**, 116621, DOI: 10.1016/j.jlumin.2019.116621.

15 H. K. Dan, D. C. Zhou, R. F. Wang, Q. Jiao, Z. W. Yang, Z. G. Song, X. Yu and J. B. Qiu, Effect of Mn^{2+} ions on the enhancement upconversion emission and energy transfer of Mn^{2+}/Tb^{3+}/Yb^{3+} tri-doped transparent glass-ceramics, *Mater. Lett.*, 2015, **150**, 76–80, DOI: 10.1016/j.matlet.2015.03.005.

16 P. X. Le, N. M. Ty, J. B. Qiu, D. C. Zhou and H. K. Dan, Enhanced upconversion and near-infrared emissions of co-doped Ho^{3+}/Yb^{3+} in TeO_2–ZnO–Na_2CO_3–La_2O_3 tellurite glasses, *Opt. Mater. Express*, 2019, **9**, 3998–4008, DOI: 10.1364/OME.9.003998.

17 A. Roy, A. Dwivedi, H. Mishra, A. K. Rai and S. B. Rai, Generation of color tunable emissions from Ho^{3+}/Tm^{3+}/Yb^{3+} co-doped $YTaO_4$ phosphors through NIR excitation under different conditions (variation of concentration, excitation pump power and the external temperature), *J. Alloys Compd.*, 2021, **865**, 158938, DOI: 10.1016/j.jallcom.2021.158938.

18 P. Dharmaiah, C. S. Dwaraka Viswanath, C. Basavapoornima, K. V. Krishnaiah, C. K. Jayasankar and S.-J. Hong, Luminescence and energy transfer in Dy^{3+}/Tb^{3+} co-doped transparent oxyfluorosilicate glass-ceramics for green emitting applications, *Mater. Res. Bull.*, 2016, **83**, 507–514, DOI: 10.1016/j.materresbull.2016.06.044.

19 H. K. Dan, N. D. Trung, T. H. Le, N. L. Thai, N. M. Ty, D. C. Zhou and J. B. Qiu, Influence of F^- on the reduction process of Eu^{3+} to Eu^{2+} and optical properties of Eu^{3+}/Eu^{2+}–Er^{3+}–Yb^{3+} co-doped niobate silicate glasses, *J. Non-Cryst. Solids*, 2022, **581**, 121417, DOI: 10.1016/j.jnoncrysol.2022.121417.

20 J. Dahiya, A. Hooda, A. Agarwal and S. Khasa, Effect of Dysprosium and Samarium RE ion co-doping on photoluminescence behaviour of novel alkali fluoride bismuth borate glasses: A white LED material, *Opt. Mater.*, 2022, **134**, 113162, DOI: 10.1016/j.optmat.2022.113162.

21 F. Nawaz, M. R. Sahar and S. K. Ghoshal, The influence of Yb co-doping on optical properties of Sm-doped sodium tellurite glasses, *Adv. Mater. Res.*, 2014, **895**, 359–362, DOI: 10.4028/www.scientific.net/AMR.895.

22 J. Li, D. Zhang, Y. X. Wu, L. L. Li, X. L. Zhang, S. Q. Xu and J. J. Zhang, Multi-color afterglow of the $LiGa_5O_8$: Tb^{3+}/Sm^{3+} co-doped gallosilicate glass *via* energy transfer and trap

sharing for optical anti-counterfeiting, *J. Mater. Chem. C*, 2024, **12**, 15733–15738, DOI: 10.1039/D4TC03171G.

23 N. Elkhoshkhany, R. Essam and E. Sayed Yousef, Influence of La_2O_3 on the structural, optical and thermal properties of TeO_2–ZnO–Li_2O–Nb_2O_5 glass, *J. Non-Cryst. Solids*, 2020, **536**, 119994, DOI: 10.1016/j.jnoncrysol.2020.119994.

24 N. Elkhoshkhany, S. Y. Marzouk, N. Moataz and S. H. Kandil, Structural and optical properties of TeO_2–Li_2O–ZnO–Nb_2O_5–Er_2O_3 glass system, *J. Non-Cryst. Solids*, 2018, **500**, 289–301, DOI: 10.1016/j.jnoncrysol.2018.08.011.

25 H. Benrejeb, K. Soler-Carracedo, A. D. Lozano-Gorrín, S. Hraiech and I. R. Martin, Energy transfer studies in Tb^{3+}–Yb^{3+} co-doped phosphate glasses, *Mater.*, 2021, **14**(22), 6782, DOI: 10.3390/ma14226782.

26 H. K. Dan, N. M. Ty, V. H. Nga, D. T. Phuc, A.-L. Phan, D. C. Zhou and J. B. Qiu, Broadband flat near-infrared emission and energy transfer of Pr^{3+}–Er^{3+}–Yb^{3+} tri-doped niobate tellurite glasses, *J. Non-Cryst. Solids*, 2020, **549**, 120335, DOI: 10.1016/j.jnoncrysol.2020.120335.

27 D. C. Zhou, R. F. Wang, Z. W. Yang, Z. G. Song, Z. Y. Yin and J. B. Qiu, Spectroscopic properties of Tm^{3+} doped TeO_2–R_2O–La_2O_3 glasses for 1.47 μm optical amplifiers, *J. Non-Cryst. Solids*, 2011, **357**, 2409–2412, DOI: 10.1016/j.jnoncrysol.2010.12.027.

28 R. El-Mallawany, Tellurite glasses Part 2. Anelastic, phase separation, Debye temperature and thermal properties, *Mater. Chem. Phys.*, 1999, **60**, 103–131, DOI: 10.1016/S0254-0584(99)00082-6.

29 G. V. Prakash, D. N. Rao and A. K. Bhatnagar, Linear optical properties of niobium-based tellurite glass, *Solid State Commun.*, 2001, **119**(1), 39–44, DOI: 10.1016/S0038-1098(01)00195-8.

30 H. K. Dan, N. M. Ty, T. D. Tap, D.-N. Le, L. T. Vinh, D. C. Zhou and J. B. Qiu, Energy transfer and spectroscopic properties of Cr^{3+}/Yb^{3+} co-doped TeO_2–ZnO–La_2O_3 tellurite glasses under different wavelength excitation lights, *Opt. Mater.*, 2020, **100**, 109662, DOI: 10.1016/j.optmat.2020.109662.

31 H. K. Dan, D. C. Zhou, R. F. Wang, T. M. Hau, Q. Jiao, Z. W. Yang, Z. G. Song, X. Yu and J. B. Qiu, Energy transfer and upconversion emission of Tm^{3+}/Tb^{3+}/Yb^{3+} co-doped transparent glass-ceramics containing Ba2LaF7 nanocrystals, *J. Non-Cryst. Solids*, 2013, **378**, 181–185, DOI: 10.1016/j.jnoncrysol.2013.07.006.

32 C. Jin, J. Zhang, W. D. Lu and Y. T. Fei, Tunable luminescence of $LiY_9(SiO_4)_6O_2$: Ce^{3+}–Tb^{3+}–Sm^{3+} phosphors for LED and temperature-sensing applications, *J. Lumin.*, 2019, **214**, 116581, DOI: 10.1016/j.jlumin.2019.116581.

33 Y. N. Guo, Q. W. Wang, X. Y. Zhao, L. P. Wang, Y. Wan, H. Zhang and C. Su, Preparation and luminescence properties of Tb^{3+}–Sm^{3+} co-doped $K_3Gd(PO_4)_2$ crystalline glass ceramics, *Opt. Mater.*, 2024, **148**, 114830, DOI: 10.1016/j.optmat.2024.114830.

34 Le-Q. Yao, G.-H. Chen, T. Yang, Y. Luo and Y. Yang, Optical properties and energy transfer in Tb^{3+}/Sm^{3+} co-doped Na_2O–CaO–P_2O_5–B_2O_3–ZrO_2 glasses, *J. Alloys Compd.*, 2017, **692**, 346–350, DOI: 10.1016/j.jallcom.2016.09.053.

35 H. K. Dan, A. L. Phan, N. M. Ty, D. C. Zhou and J. B. Qiu, Optical bandgaps and visible/near-infrared emissions of Bi^{n+}-doped (n = 1, 2, and 3) fluoroaluminosilicate glasses *via* Ag^{+}–K^{+} ions exchange process, *Opt. Mater.*, 2021, **112**, 110762, DOI: 10.1016/j.optmat.2020.110762.

36 P. T. Phong, P. H. Nam, N. X. Phuc, B. T. Huy, L. T. Lu, D. H. Manh and I.-J. Lee, Effect of zinc concentration on the structural, optical, and magnetic properties of mixed Co–Zn ferrites nanoparticles synthesized by low-temperature hydrothermal method, *Metall. Mater. Trans. A*, 2019, **50**, 1571–1581, DOI: 10.1007/s11661-018-5096-z.

37 K. A. Kumar, S. Babu, V. R. Prasad, S. Damodaraiah and Y. C. Ratnakaram, Optical response and luminescence characteristics of Sm^{3+} and Tb^{3+}/Sm^{3+} co-doped potassium-fluoro-phosphate glasses for reddish-orange lighting applications, *Mater. Res. Bull.*, 2017, **90**, 31–40, DOI: 10.1016/j.materresbull.2017.01.046.

38 V. Lakkamraju, K. N. Kumar and H. Pyung, Unravelling the process of energy transfer and color tuning from warm to cool white light emission in (Tb/Sm): lithium borate glasses, *Opt. Lett.*, 2019, **44**(20), 5029–5032, DOI: 10.1364/OL.44.005029.

39 C. G. Pérez-Hernández, R. Sánchez-Zeferino, U. Salazar-Kuri and M. E. Álvarez-Ramos, Fabrication, structural properties, and tunable light emission of Sm^{3+}, Tb^{3+} co-doped $SrSnO_3$ perovskite nanoparticles, *Chem. Phys.*, 2021, **551**, 111324, DOI: 10.1016/j.chemphys.2021.111324.

40 A. Bahadur, R. S. Yadav, R. V. Yadav and S. B. Rai, Multimodal emissions from Tb^{3+}/Yb^{3+} co-doped lithium borate glass: upconversion, downshifting and quantum cutting, *J. Solid State Chem.*, 2017, **246**, 81–86, DOI: 10.1016/j.jssc.2016.11.004.

41 S. Pandey, A. Pandey and V. K. Rai, Synthesis and Characterization of Sm^{3+}–Yb^{3+} codoped Y_2O_3 Phosphor, *J. Disp. Technol.*, 2013, **9**(12), 989–994. https://doi:10.1016/s0038-1098(01)00195-8.

42 T. T. Hong, P. D. H. Yen, V. X. Quang and P. T. Dung, Luminescence properties of Ce/Tb/Sm co-doped tellurite glass for white LEDS application, *Mater. Trans.*, 2015, **56**(9), 1419–1421, DOI: 10.2320/matertrans.MA201509.

43 Y. Z. Jiang, H. P. Xia, L. Fu, J. Z. Zhang, S. Yang, X. M. Gu, J. L. Zhang, Y. P. Zhang, D. J. Wang, H. C. Jiang and B. J. Chen, Growth and Optical Spectra of Tb^{3+}/Sm^{3+}/Ce^{3+} Triply doped $LiYF_4$ single crystals for White-Light LEDs, *Nanosci. Nanotechnol.*, 2016, **16**, 1532–1536, DOI: 10.1166/jnn.2016.10803.

44 X. K. Sun, Z. Z. Huang, Y. H. Guo, S. H. Zhou and K. L. Liu, $Tb^{3+} \rightarrow Sm^{3+}$ energy transfer induced tunable luminescence in $Ba_3MgSi_2O_8$:Tb^{3+}/Sm^{3+} phosphors, *J. Lumin.*, 2020, **219**, 116925, DOI: 10.1016/j.jlumin.2019.116925.

45 A. N. Meza-Rocha, G. Muñoz H, A. Speghini, M. Bettinelli and U. Caldiño, Neutral and warm white light emission in Tb^{3+}/Sm^{3+} zinc phosphate glasses, *Opt. Mater.*, 2015, **47**, 537–542, DOI: 10.1016/j.optmat.2015.06.035.

46 N. F. Andrade Neto, J. M. P. Silva, R. L. Tranquilin, E. Longo, J. F. M. Domenegueti, M. R. D. Bomio and F. V. Motta, Photoluminescent properties of Sm^{3+} and Tb^{3+} codoped

$CaWO_4$ nanoparticles obtained by a one-step sonochemical method, *J. Mater. Sci.: Mater. Electron.*, 2020, **31**, 13261–13272, DOI: 10.1007/s10854-020-03878-7.

47 K. Nie, R. R. Zhou, C.-A. Cheng, X. Q. Duan, Z. Y. Hu, L. F. Mei, H. K. Liu, L. X. Wang, H. Wang and X. X. Ma, Tb^{3+} and Sm^{3+} co-doped $Ca_2La_3(SiO_4)_3F$ phosphor: Synthesis, color regulation, and luminescence properties, *RSC Adv.*, 2022, **12**, 33200–33206, DOI: 10.1039/D2RA06648C.

48 B. Yuan, J. X. Gou, C. C. Qi, L. Kong, M. Y. Qu, G. Y. Luan and X. T. Zhang, Energy transfer for $Ce^{3+}/Tb^{3+}/Sm^{3+}$ induced bright white emission in single-phase $CaLa_4(SiO_4)_3O$: Ce^{3+}, Tb^{3+}, Sm^{3+} phosphors and their application in white-light-emitting diodes, *RSC Adv.*, 2024, **14**, 7061–7072, DOI: 10.1039/D4RA00443D.

49 Y. N. Guo, Q. W. Wang, X. Y. Zhao, L. P. Wang, Y. C. Wan, H. B. Zhang and C. H. Su, Preparation and luminescence properties of Tb^{3+}-Sm^{3+} co-doped $K_3Gd(PO_4)_2$ crystalline glass ceramics, *Opt. Mater.*, 2024, **148**, 114830, DOI: 10.1016/j.optmat.2024.114830.

50 E. J. Ansari, S. Patle, A. R. Pusdekar, N. S. Ugemuge and A. Selokar, Structural and spectroscopic analysis of $K_2Y(WO_4)(PO_4)$: Sm^{3+}, Tb^{3+} phosphors for optical applications, *Spectrochim. Acta Part A Mol. Spectrosc.*, 2025, 126269, DOI: 10.1016/j.saa.2025.126269,https://www.sciencedirect.com/journal/spectrochimica-acta-part-a-molecular-and-biomolecular-spectroscopy/vol/339/suppl/C339.

51 O. Soriano-Romero, E. F. Huerta, A. N. Meza-Rocha and U. Caldiño, Orange and yellow emissions through Sm^{3+} and Tb^{3+}/Sm^{3+} doped potassium-zinc phosphate glasses for WLED applications, *Ceram. Interfaces*, 2023, **49**, 36353–36359, DOI: 10.1016/j.ceramint.2023.08.319.

52 J. Hernández-Andrés, R. L. Lee and J. Romero, Calculating correlated color temperatures across the entire gamut of daylight and skylight chromaticities, *Appl. Opt.*, 1999, **38**(27), 5703–5709, DOI: 10.1364/AO.38.005703.

53 M. E. Alvarez-Ramos, J. Alvarado-Rivera, M. E. Zayas, U. Caldiño and J. Hernández-Paredes, Yellow to orange-reddish glass phosphors: Sm^{3+}, Tb^{3+} and Sm^{3+}/Tb^{3+} in zinc tellurite-germanate glasses, *Opt. Mater.*, 2018, **112**, 88–93, DOI: 10.1016/j.optmat.2017.09.033.

54 X. S. Qiao, X. P. Fan, Z. Xue and X. H. Xu, Short-wavelength upconversion luminescence of Yb^{3+}/Tm^{3+} co-doped glass ceramic containing SrF_2 nanocrystals, *J. Non-Cryst. Solids*, 2011, **357**(1), 83–87, DOI: 10.1016/j.jnoncrysol.2010.09.008.

55 D. T. Khan, N. T. Dang, S. H. Jabarov, T. G. Naghiyev, R. M. Rzayev, T. Q. Nguyen, H. V. Tuyen, N. T. Thanh and L. V. T. Son, Study on luminescent properties of Tb^{3+} and Sm^{3+} co-doped CaSiO3 phosphors for white light emitting diodes, *Mater. Res. Express*, 2020, **7**, 016507, DOI: 10.1088/2053-1591/ab5ab8.